Supporting Information for "Evidence of subduction related thermal and compositional heterogeneity below the United States from transition-zone receiver functions"

Ross Maguire,[1] Jeroen Ritsema,[1] Saskia Goes,[2]

Contents of this file

1. Text S1

2. Figures S1 to S6

Introduction

This supplemental material includes a description of synthetic tests to check for imaging artifacts due to incomplete data coverage and the influence of heterogeneous crust.

---

[1]Department of Earth and Environmental Sciences, University of Michigan, Ann Arbor, MI, 48109-1005, USA

[2]Department of Earth Science and Engineering, Imperial College London, London, SW7 2AZ, United Kingdom

Additionally, we discuss how we infer the temperature and composition of the transition zone from mineral physics based velocity models of mechanical mixtures of basalt and harzburgite. Finally, we illustrate the sensitivity of the common conversion point images to the 3D seismic velocity model used for migration. We include 6 additional figures, described in Text S1.

Text S1. Receiver function imaging of velocity gradients in the upper mantle is complicated by the non uniform distribution of earthquakes and seismic stations. The imperfect illumination hampers resolution of discontinuity topography and may introduce artifacts such as artificial duplexing of seismic interfaces [e.g., *Lekić and Fischer*, 2017].

In this study, we analyze teleseismic earthquakes with magnitudes $6 \leq M_w \leq 7$ recorded by the US Transportable array (Figure 1A). The dataset includes seismograms from 222 earthquakes that occurred between 2008 and 2014. The station spacing of the USArray is less than 100 km on average. The range of epicentral distances is relatively uniform (Figure 1B) but the back-azimuth distribution is bimodal since the majority of earthquakes occurred in the western Pacific and South America (Figure 1C).

To test for artifacts due to illumination geometry, we apply all receiver function processing steps to synthetic seismograms for each of the events used in the study. We compute these synthetic waveforms at frequencies as high as 0.2 Hz using the spectral element method waveform solver AxiSEM [*Nissen-Meyer et al.*, 2014], for source parameters documented in the Global CMT catalog [*Ekström et al.*, 2012], and for the AK135 seismic reference model [*Montagner and Kennett*, 1996]. The set of synthetic receiver functions has an identical ray parameter and back azimuth distribution as the observational data,

and is affected by deconvolution in a similar manner. Since AK135 includes only the 410 and 660 discontinuities we expect only P410s and P660s wave conversions to appear in our synthetic CCP images.

Figure 2 shows slices of the synthetic receiver function stacks along transects X, Y, and Z (as in Figure 1 in the main text). The 410 and 660 are the primary features in each cross section. The amplitudes of P410s and P660s are relatively uniform across the imaging region, suggesting these discontinuities are well resolved in our study. Signals from the 520 and 730 are absent in the synthetics likely indicating that our observations of $P520s$ and $P730s$ are not artifacts from poor wave coverage. The complex signals between 250 and 400 km depth are conversions from shallower gradients and their reverberations. The broadening of P410s and the high-amplitude signal near 300 km depth in cross section Z near $-120°$ longitude are due to poor data coverage near the eastern and western boundaries of the cross sections.

The crust adds additional complexity in receiver functions since reverberations within the crust can masquerade as P-to-S conversions from discontinuities in the mantle. Crustal reverberations are expected to be strongest in regions with thick low velocity layers such as sedimentary basins. We test the influence of crustal reverberations by forward calculating receiver function stacks for AK135 with and without a crust.

The synthetic receiver functions are based on AxiSEM synthetics with a minimum period of 5 s. They are calculated at stations with epicentral distances between 30–90°. We use the crustal profile 'DN' from CRUST2.0 [*Laske et al.*, 2001], which characterizes the crustal structure over broad regions of the southeastern US near the Gulf of Mexico,

where we detect the strongest $P730s$. The upper 6 km of DN has two sedimentary layers with shear velocities of 1.2 km/s and 2.4 km/s. Figure 3A shows the velocity structure of AK135 (green) and AK135 with crustal model DN included (blue).

Figures 3B and 3C show stacked receiver functions for AK135 and AK135 with profile DN added, respectively. In Figure 3C, weak arrivals about 8.7 s after P410s and P660s are reverberations within the low velocity crust. The amplitude of the crustal reverberations is much smaller than the P520s and P730s phases observed in the Gulf of Mexico region (Figure 3D). Additionally, Figure 3D shows that the time between $P410s$ and $P520s$ (i.e., 9.8 s) is not the same as the time between $P660s$ and $P730s$ (i.e., 5.5 s). If the detected $P520s$ and $P730s$ phases were misidentified crustal reverberations, they should be recorded after their parent phases with the same delay of about 8.7 s. More complex crustal structure, beyond the simple 1D model we consider here, could potentially influence receiver function stacks in unknown ways. Complimentary transition zone imaging techniques such as ScS reverberations and SS precursors could be used to validate our observations of $P730s/P660s$ amplitude ratios, but we leave this to future work.

In this study, our interpretations of the temperature and composition of the MTZ are based on theoretical seismic velocity profiles of mechanical mixtures of basalt and harzburgite. To relate the seismic velocity profiles to observed receiver function stacks, we calculate synthetic receiver function stacks for mechanical mixtures with varying basalt fraction f and potential temperature (i.e., each of the seismic velocity profiles shown in Figure 3A and 3C of the main text). As before, stacks are computed using AxiSEM synthetics accurate to a minimum period of 5 s.

Figure 4A shows synthetic receiver function stacks for varying potential temperature with a fixed composition of $f = 0.2$ (i.e., a roughly pyrolitic composition). The time between $P410s$ and $P660s$ determines the temperature in the transition zone (Figure 4A, main text). Figures 4B – F show synthetic receiver function stacks calculated for mechanical mixtures with variable f and potential temperatures ranging between 1200 K and 1600 K. When $f = 0$ (i.e., pure harzburgite) the $P410s$, $P520s$, and $P660s$ are strong. As f increases, these phases decrease in amplitude, but $P730s$ increases in amplitude. When $f = 1$ (i.e., pure basalt), $P730s$ is the only arrival near the base of the transition zone. We use the amplitude ratio of $P730s$ to $P660s$ (as shown in Figure 3B, main text) to create maps of basalt fraction at the base of the transition zone (i.e., Figure 4C, main text). The synthetic P730s/P660s amplitude ratios are only very weakly sensitive to temperature. The map in Figure 4C is based on synthetic amplitude ratios computed for a 1300 K adiabat.

We investigate the influence of the velocity model on estimates of transition zone thickness and temperature by migrating the receiver functions with three different models. These models are AK135, US-SL-2014 [*Schmandt and Lin*, 2014a], and DNA13 [*Porritt et al.*, 2014]. Figure 5 shows a comparison of MTZ temperature and thickness for each of the models. The strong agreement in the pattern of transition zone thickness indicates that our results are robust. However, adding the 3D corrections can modify the estimates of transition zone thickness by 10 km or more in some regions. For example, when 3D corrections are not applied (Figure 5A), much of the eastern US is characterized by a transition zone with approximately normal thickness ($\sim$ 250 km). However, when Pds travel

times are corrected for 3D velocity variations (Figures 5B and C) a thicker than average transition zone is revealed in regions where slab fragments are imaged at transition zone depths.

Figure 6 shows the absolute depths of the 410 and 660 imaged using AK135 (Figure 6 A and C), and US-SL-2014 (Figure 6B and D). When no 3D corrections are applied, the deflections of the 410 and 660 are strongly correlated. Below the western US, the slow velocities in the upper mantle cause a downward deflection of both the 410 and 660. The opposite is true below the much of the eastern US due to positive velocity anomalies. The correlations are not as clear when 3D corrections are applied.

References

Ekström, G., M. Nettles, and A. M. Dziewoński (2012), The global CMT project 2004 2010 : Centroid-moment tensors, *Physics of the Earth and Planetary Interiors*, *201*, 1–9, doi:10.1016/j.pepi.2012.04.002.

Laske, G., G. Masters, and C. Reif (2001), Crust2. 0: a new global crustal model at 2× 2 degrees, *Institute of Geophysics and Planetary Physics, The University of California, San Diego, website http://mahi. ucsd. edu/Gabi/rem. dir/crust/crust2. html*.

Lekić, V., and K. M. Fischer (2017), Interpreting spatially stacked Sp receiver functions, *Geophysical Journal International*, *210*(2), 874–886, doi:10.1093/gji/ggx206.

Montagner, J.-P., and B. L. N. Kennett (1996), How to reconcile body-wave and normal-mode reference earth models, *Geophysical Journal International*, *125*(1), 229–248, doi:10.1111/j.1365-246X.1996.tb06548.x.

Nissen-Meyer, T., M. Van Driel, S. C. Stähler, K. Hosseini, S. Hempel, L. Auer, A. Colombi, and A. Fournier (2014), AxiSEM: Broadband 3-D seismic wavefields in axisymmetric media, *Solid Earth*, *5*(1), 425–445, doi:10.5194/se-5-425-2014.

Porritt, R. W., R. M. Allen, and F. F. Pollitz (2014), Seismic imaging east of the Rocky Mountains with USArray, *Earth and Planetary Science Letters*, *402*(C), 16–25, doi:10.1016/j.epsl.2013.10.034.

Schmandt, B., and F.-c. Lin (2014a), P and S wave tomography of the mantle beneath the United States, *Geophysical Research Letters*, *41*, 6342–6349, doi:10.1002/2014GL061231.

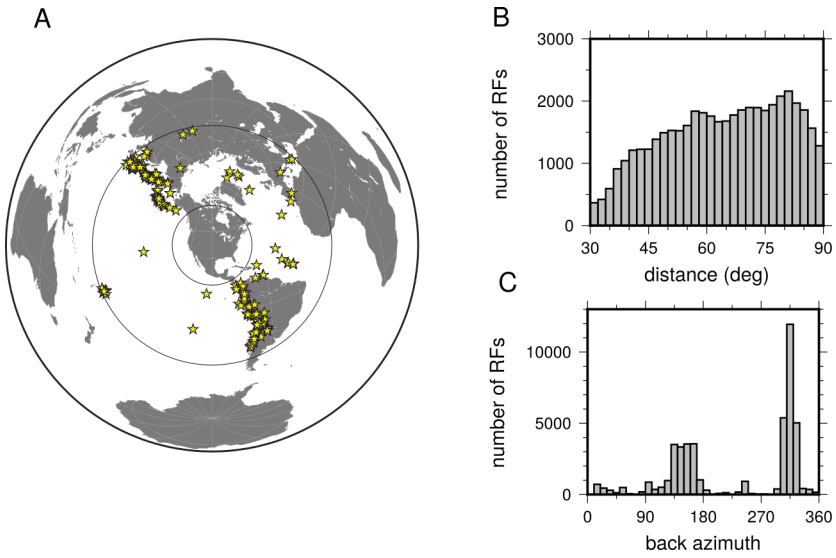

Figure 1. (A) Epicenters of events used in this study. (B) The distribution of epicentral distances. (C) the distribution of back azimuths.

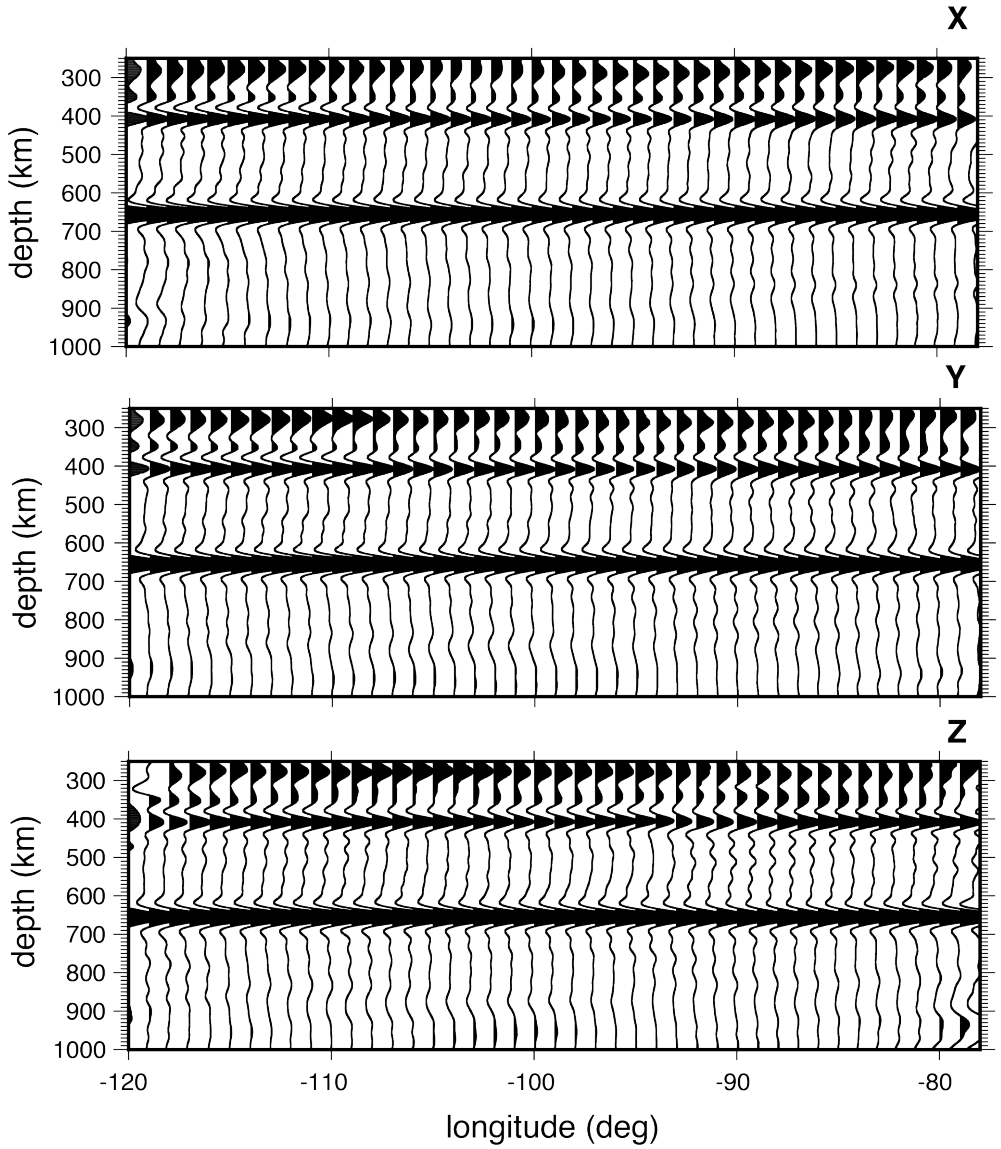

Figure 2. Cross sections through synthetic CCP image at latitudes of 44° (cross section X), 38° (cross section Y), and 32° (cross section Z). The CCP image is based on synthetic receiver functions for seismic model AK135 with discontinuities at 410 km and 660 km depth only. Compare to Figure 1 in main text.

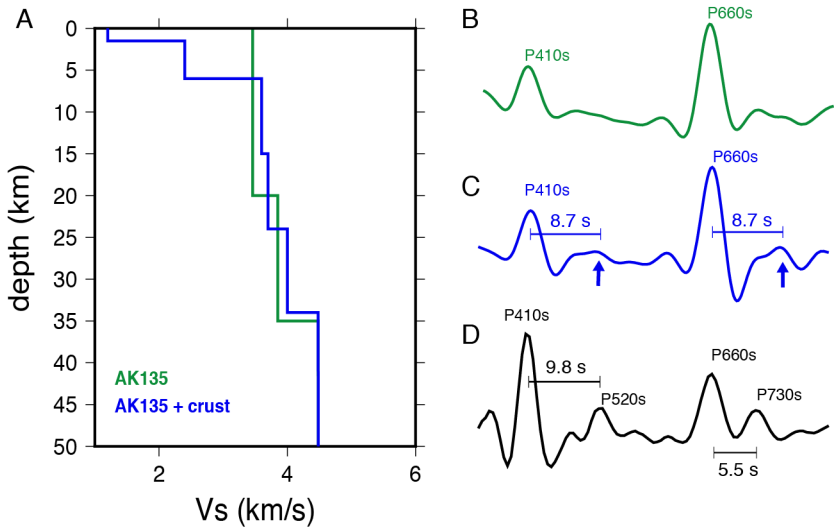

Figure 3. (A) Profiles of V_S for AK135 (in green) and AK135 plus crustal profile DN from CRUST2.0 (in blue). (B) and (C) show synthetic receiver function stacks computed for these two profiles. In (C), weak positive arrivals about 8.7 s after both P410s and P660s (marked with arrows) are crustal reverberations. (D) shows a vertical profile of the CCP image in the southeast US, near the Gulf of Mexico (a location characterized by DN in CRUST2.0). P-to-S conversions from P410s, P520s, P660s, and P730s are labeled.

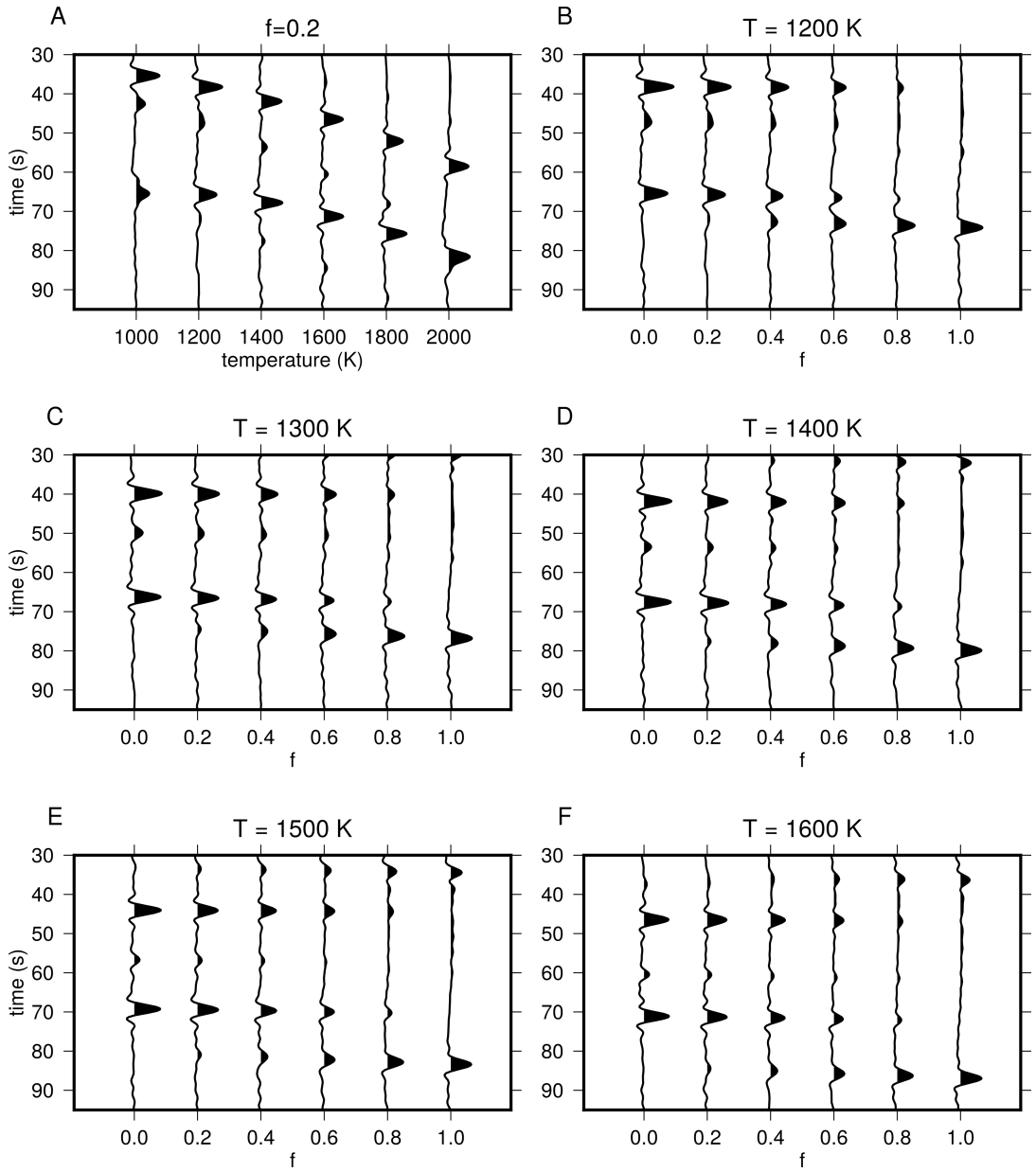

Figure 4. Synthetic receiver functions calculated for mineral-physics based velocity models. (A) Receiver function stacks for a mantle with $f = 0.2$ for potential temperatures ranging between 1000 K and 2000 K. (B – F) Receiver function stacks for a mantle with varying f. The potential temperatures range between 1200 K and 1600 K.

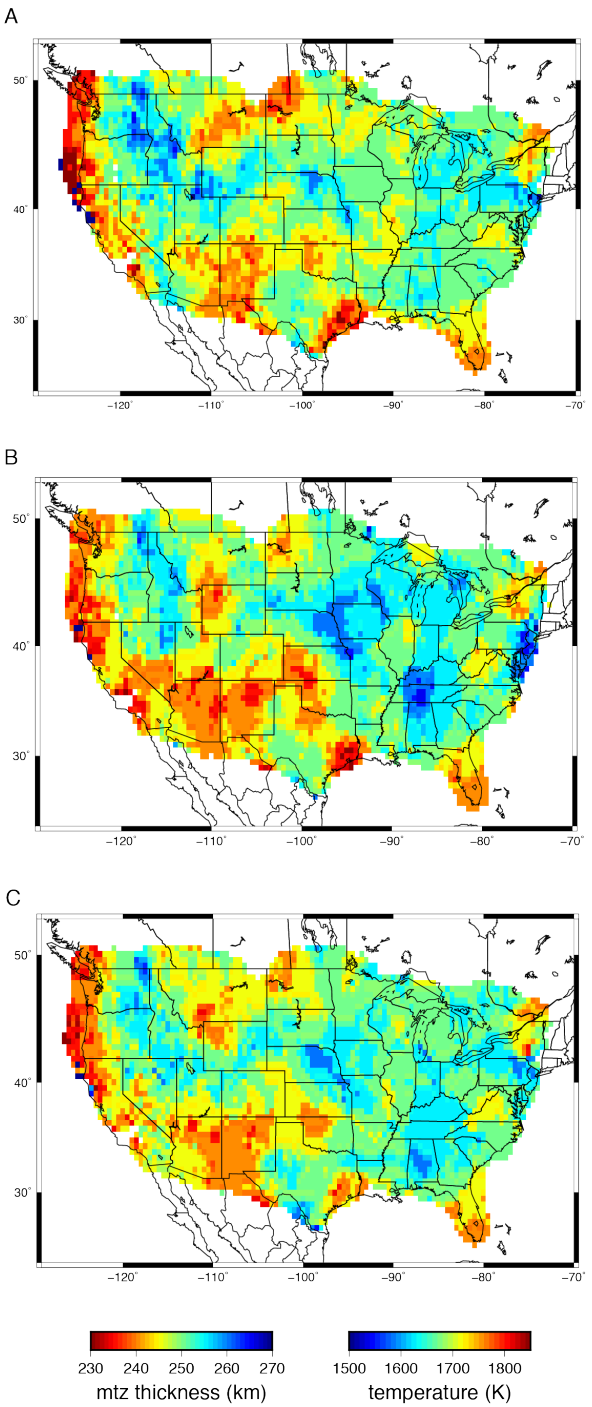

Figure 5. Comparison of mantle transition zone thickness maps created assuming different mantle velocity structures. Map A uses AK135 to migrate receiver functions to depth. Maps B and C use 3D tomography models US-SL-2014 (Schmandt and Lin, 2014), and DNA13 (Porritt et al., 2014), respectively.

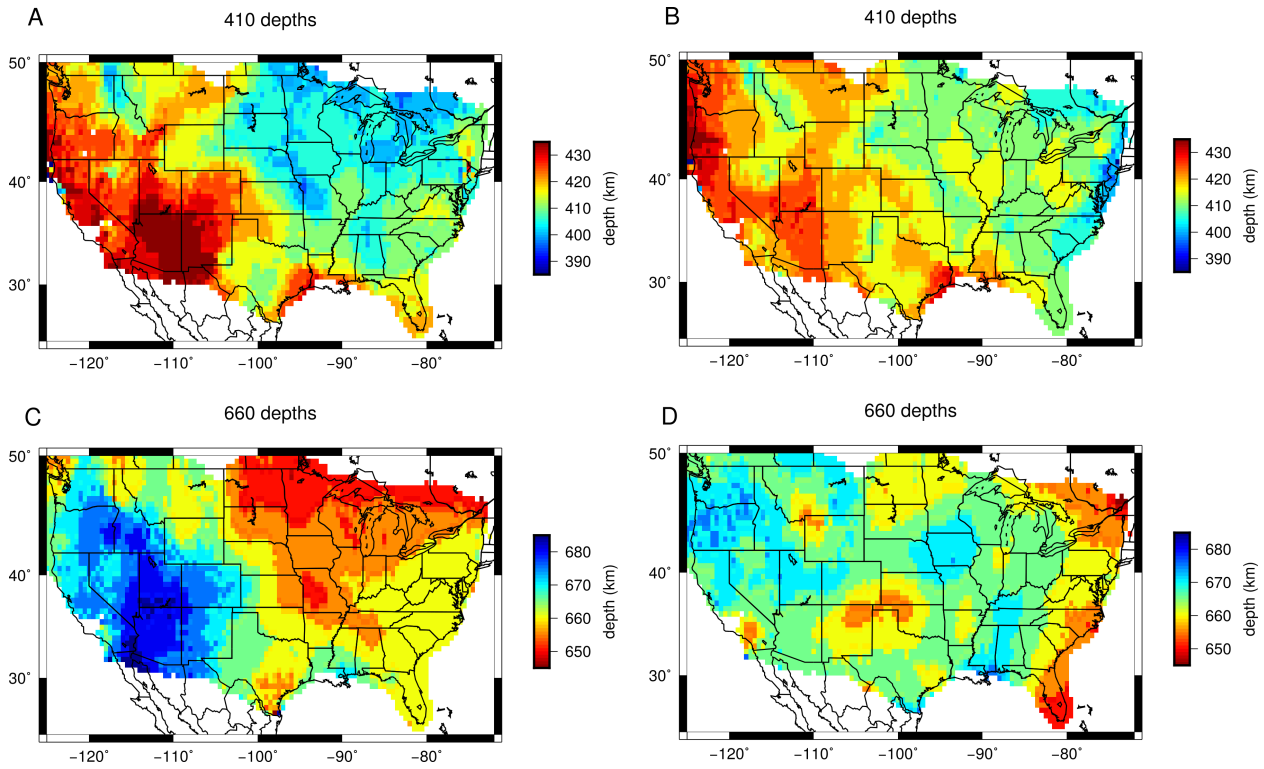

Figure 6. Imaged depths of the 410 and 660 discontinuities using AK135 (A and C), and using the 3D velocity model US-SL-2014 (B and D).